Collisional relaxation of excited-state Zeeman coherences in atomic ytterbium vapor

A. G. Yodh, J. Golub, and T. W. Mossberg
Department of Physics, Harvard University, Cambridge, Massachusetts 02138
(Received 19 November 1984)

We present the results of an experiment designed to probe the collision-induced relaxation of excited-state Yb Zeeman coherences. Our experiment is sensitive not only to the depolarization-type relaxation mechanisms often observed in optical-pumping experiments, but also to the effects of collisionally induced velocity changes. Our measurements were performed in the $6s\,6p\ ^3P_1$ excited state of the even ($I=0$) isotopes of gas-phase atomic Yb by means of a trilevel photon-echo technique. Depolarization rates, velocity-change spectra, and total scattering cross sections of Yb-He (Yb-Ar) collisions were measured (deduced). Both rank-1 and rank-2 spherical tensor components of the $^3P_1$ state play a role in our experiment, and our results represent averages of potentially different relaxation rates attributable to these quantities. Comparison of our results with rank-0 results obtained elsewhere reveals interesting similarities as well as differences.

I. INTRODUCTION

The collisional relaxation of Zeeman coherences is a particularly fascinating subject, and has been of interest for many years.[1] One of the reasons for this interest is that a given Zeeman manifold may exhibit a number of distinct relaxation rates corresponding to the various ranks of spherical tensors needed to describe the manifold.[2–4] Optical-pumping experiments have provided a wealth of data on the relaxation of Zeeman coherences induced by collisional depolarization (i.e. population thermalization). Until recently, however, little data was available[5–9] concerning the relaxation of Zeeman coherences by collision-induced velocity changes.[10–13] The present work is one of the first experiments sensitive to the entire spectrum of velocity changes affecting a particular active atom-perturber system. By comparing our results with those obtained in other recent experiments,[6,7] interesting insights into the response of different spherical tensor moments to velocity changes are obtained.

Recently, it has been demonstrated that photon-echo techniques are well suited to the study of collisionally-induced velocity changes affecting either coherences or populations.[5,6,14–18] We have employed a particular echo technique, a trilevel photon echo,[19] to study the He- and Ar-induced collisional relaxation of Zeeman coherences in the $6s\,6p\ ^3P_1$ excited-state of atomic Yb. From our measurements we were able to make reasonable estimates of the depolarizing and the velocity-changing collision cross sections for Yb* in He and Ar. (Here and henceforth Yb* denotes excited-state Yb.) We have also determined phenomenological velocity-changing kernels (velocity-change spectra) for these scattering processes. By varying the temporal separation of our excitation pulses we were able to study both the effects of strong collisions and weak, diffractive collisions.

This paper is organized as follows. We first give a brief theoretical discussion of the trilevel echo technique and its use in measuring collisional relaxation. Then we describe our experiment. Finally we present and discuss our results. In particular, we compare our results with Yb*-collision data measured elsewhere which are sensitive to different spherical tensor moments than ours.

II. THEORY

We first outline the formation of the trilevel echo signal employed in our measurements. More detailed discussions of trilevel echo formation can be found elsewhere.[19,20]

An energy-level diagram appropriate to our experimental conditions is given in Fig. 1. We quantize along $\hat{\mathbf{z}}$ and have all excitation pulses propagating along $\hat{\mathbf{y}}$. Three excitation pulses having the linear polarizations shown in Fig. 2(a) are applied. The pulses are assumed to have the form

$$E_p(\mathbf{r},t)=\mathscr{E}_p(t-\eta_p)\exp(-i\{\omega_p[t-\eta_p(\mathbf{r})]+\varphi_p\})\ , \qquad (1)$$

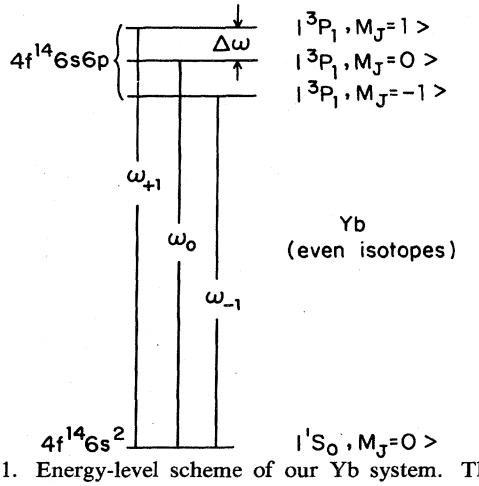

FIG. 1. Energy-level scheme of our Yb system. This diagram describes the nuclear-spin zero, even isotope-level structure. The excited-state m levels are split by a small magnetic field applied in the $\hat{\mathbf{z}}$ direction. (See text.)

where $p=1, 2, 3$, $\eta_p(\mathbf{r})=\hat{\mathbf{k}}_p\cdot(\mathbf{r}-\mathbf{r}_0)/c+t_p$, $\mathbf{k}_p$ is the wave vector of pulse p, $\mathbf{r}_0$ is the center of the Yb-vapor cell, and t_p is the time that pulse p reaches $\mathbf{r}_0$. We assume that the pulses are sufficiently brief that they can be treated as exactly resonant with all atoms involved.

Let us consider the evolution of the atomic wave function $\psi(t)$ under the influence of the resonant pulses in Fig. 2(a). The effect of pulse one is to create an optical coherence between the states $|{}^1S_0,0\rangle$ and $|{}^3P_1,0\rangle$ (see Fig. 2). The second pulse excites the $|{}^1S_0,0\rangle$-$|{}^3P_1,\pm1\rangle$ transitions. As a result, phase information stored in the optical coherence is transferred to Zeeman coherences.[19] After pulse two, $\psi(t)$ consists of a superposition of excited-state m levels. The wave function may, in general, also contain a ground-state term, but in our case the trilevel echo amplitude is only sensitive to the excited-state terms.[20] It is relatively straightforward to show that for $t_2<t<t_3$, the excited-state component of a particular atom's wave function is given by[19]

$$\psi(t)=iS_1\exp(-i\{\omega_0[t-\eta_1(\mathbf{r}_1)]+\varphi_1\})\,|{}^3P_1,0\rangle + \frac{i}{\sqrt{2}}S_2C_1[\exp(-i\{\omega_{-1}[t-\eta_2(\mathbf{r}_2)]+\varphi_2\})\,|{}^3P_1,-1\rangle-\exp(-i\{\omega_{+1}[t-\eta_2(\mathbf{r}_2)]+\varphi_2\})\,|{}^3P_1,+1\rangle]\,, \tag{2}$$

where $S_p=\sin(\frac{1}{2}\theta_p)$, $C_p=\cos(\frac{1}{2}\theta_p)$, θ_p is the area of the pth pulse defined in *each* case using the matrix element appropriate to the $|{}^1S_0,0\rangle$-$|{}^3P_1,0\rangle$ transition, ω_{-1}, ω_0, and ω_{+1} are the angular frequencies corresponding to transitions from the $|{}^1S_0,0\rangle$ state to the $|{}^3P_1,-1\rangle$, $|{}^3P_1,0\rangle$, and $|{}^3P_1,1\rangle$ states, respectively. We allow these frequencies to differ so that our calculation can account for the effects of a weak magnetic field. The symbol $\eta_p(\mathbf{r}_p)$ gives the time that the atom was excited by pulse p. Here $\mathbf{r}_p$ is the position occupied by the atom at the time it is excited by pulse p. We will return to examine this wave function shortly.

At $t=t_3$, pulse three transfers population from the $|{}^3P_1,0\rangle$ state to the $|{}^1S_0,0\rangle$ state creating optical coherences between the states $|{}^1S_0,0\rangle$ and $|{}^3P_1,\pm1\rangle$. At $t_e=t_3+t_{21}$, where $t_{ij}=t_i-t_j$, this coherence rephases, giving rise to an echo polarized in the $\hat{\mathbf{x}}$ direction. Thus we see that the echo signal depends on the persistence of Zeeman (optical) coherences during t_{32} (t_{21} and t_{e3}). Atoms that undergo collisions between t_1 and t_e in general suffer perturbations, which limit the extent to which the affected atoms can participate in the emission of the echo signal. The echo intensity is correspondingly decreased.

In the present work we are interested in the relaxation of the Zeeman coherences during t_{32}. We can qualitatively understand why our experiment is sensitive to velocity changes by considering the atomic wave function and the observables that can be derived from it during t_{32}. If an atom's velocity $\mathbf{v}$ can be regarded as constant, we can express the position of the atom during pulse p in terms of its position $\mathbf{r}$ at some arbitrary time t by

$$\mathbf{r}_p=\mathbf{r}-\mathbf{v}(t-t_p)\,. \tag{3}$$

Using the fact that $\mathbf{k}\|\hat{\mathbf{y}}$, we can rewrite the excited-state wave function of Eq. (2) which is a function of $\mathbf{r}_1$, $\mathbf{r}_2$, and t so that it is instead a function of y, v_y, and t, i.e.,

$$\psi(t,v_y,y)=iS_1\exp\{-i[\omega_0(t-t_1)-k_0(y-y_0)+k_0v_y(t-t_1)+\varphi_1]\}\,|{}^3P_1,0\rangle + \frac{i}{\sqrt{2}}S_2C_1(\exp\{-i[\omega_{-1}(t-t_2)-k_{-1}(y-y_0)+k_{-1}v_y(t-t_2)+\varphi_2]\}\,|{}^3P_1,-1\rangle - \exp\{-i[\omega_1(t-t_2)-k_1(y-y_0)+k_1v_y(t-t_2)+\varphi_2]\}\,|{}^3P_1,1\rangle)\,. \tag{4}$$

Here k_1, k_0, and k_{-1} are equal to ω_1/c, ω_0/c, and ω_{-1}/c, respectively. Using $\psi(t,v_y,y)$ to calculate the orientation and alignment associated with the $^3P_1$ Zeeman manifold, one finds that these quantities are modulated in amplitude as a function of v_y. Consider, for example, the y component of the sample's magnetization which is proportional to the expectation value of J_y. It is straightforward to show that

$$m_y(v_y)\propto\langle\psi\,|\,J_y\,|\,\psi\rangle=-2C_1S_1S_2\sin[v_yk_0t_{21}+\omega_0t_{21}-(\varphi_2-\varphi_1)]\cos\left[\Delta\omega\left[t-t_2-\frac{y-y_0}{c}\right]\right]\,, \tag{5}$$

where $\Delta\omega\equiv\omega_1-\omega_0=\omega_0-\omega_{-1}$. The magnetization oscillates as a function of v_y with a period given by

$$v_{\mathrm{mod}}=\frac{2\pi}{k_0t_{21}}=\frac{\lambda_0}{t_{21}}\,.$$

This period can be varied simply by changing t_{21}. In the Appendix we analyze the formation of our echo signal in terms of spherical tensors. We find that the echo signal depends on a velocity modulation in the spherical tensors ρ_1^1 (a component of orientation) and ρ_1^2 (a component of alignment). This velocity dependence has the same qualitative form as shown in Eq. (5). The collisionally induced velocity-change spectrum is studied by varying t_{21} and hence v_{mod}. When a collision perturbs v_y by an amount small compared to v_{mod} it contributes only weakly to collisional degradation of the echo (see below).

In the analysis of collisional relaxation of optical transitions,[14] it is typical to divide the effects of collisions into three categories. These are inelastic, phase changing, and

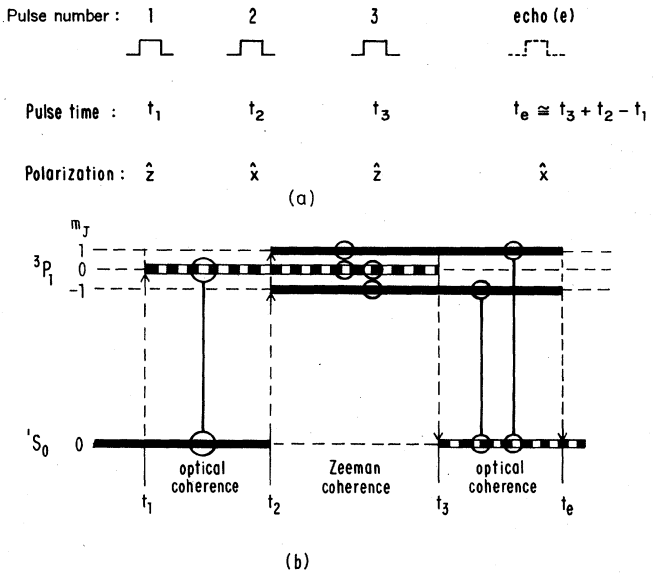

FIG. 2. Excitation pulses and level coherences involved in the trilevel echo effect used here. (a) The trilevel echo excitation-pulse sequence. The polarization direction of each pulse is indicated below the pulse time. Note that pulses propagate in the $\hat{y}$ direction, and that a small magnetic field is applied along our quantization axis $\hat{z}$. We have also indicated the polarization, and emission time of the trilevel echo induced by the first three pulses. (b) The level coherences important at various times before emission of the trilevel echo. Heavy dashed and solid horizontal lines indicate a level population important in the echo evolution process at a given time. Vertical lines terminating in open circles indicate the important coherences. The two Zeeman coherences important during the central interval exhibit velocity modulation. (See text.)

velocity changing. In the case of Zeeman coherences, the first two processes can no longer be considered distinct. This results from the fact that spatial rotations can transform what appear to be Zeeman coherences (off-diagonal density-matrix elements) into Zeeman populations (diagonal density-matrix elements) and vice versa. As a result, all collisional perturbations of the internal state of a particular atom's Zeeman manifold are lumped under the title of depolarization effects. Depolarization effects reduce the *magnitude* associated with various spherical tensor components. These effects occur primarily in strong close-encounter collisions. In weak collisions, on the other hand, the internal state of the atom remains essentially unchanged, but the atom as a whole experiences a velocity change. These velocity changes reduce the velocity modulation associated with various spherical tensor components. Both depolarizing and velocity-thermalizing collisional perturbations contribute to relaxation of the trilevel echo signal.

The effects of depolarizing and velocity-changing collisions, taken together, lead to a simple exponential decay of echo intensity as a function of perturber pressure. At fixed-pulse separations and in the binary collision approximation, the trilevel echo intensity will decay with perturber-gas pressure as[19,20]

$$I_e(P)=I_0\exp[-\beta(t_{21},t_{32})P]$$
$$=I_0\exp[-\beta_{\rm opt}(t_{21})P]\exp[-\beta_z(t_{21},t_{32})P]\ . \quad (6)$$

Here $\beta_{\rm opt}(\beta_z)$ represents the decay constant that arises from collisional effects on the optical coherences (Zeeman coherences). Since $\beta_{\rm opt}$ is independent of t_{32}, and (as will be seen from the equations below) β_z varies linearly with t_{32}, measurements of β for several values of t_{32} for each t_{21} allow us to determine $\beta_{\rm opt}$ (t_{21}), and β_z (t_{21},t_{32}) separately. The optical coherence measurements obtained in the course of our experiment were consistent with those presented elsewhere and will be discussed no further.[15] Henceforth we will concentrate solely on the Zeeman relaxation.

Assuming that the collisions are randomly distributed in time and are binary, one can show that[19]

$$\beta_z=\frac{2n_0}{P_0}v_{\rm rel}t_{32}\left[\sigma_D^z+\sigma_{vcc}^z\left[1-\int_{-\infty}^{\infty}W(\Delta v_y)\exp(ik\,\Delta v_y\,t_{21})d(\Delta v_y)\right]\right]=\frac{2n_0}{P_0}v_{\rm rel}t_{32}\sigma_{\rm eff}^z(t_{21})\ , \quad (7)$$

where σ_D^z is the cross section for depolarizing collisions, σ_{vcc}^z is the cross section for collisions that produce velocity changes but do not depolarize, $W(\Delta v_y)$ is a scattering kernel, assumed symmetric about $\Delta v_y=0$, which gives the probability that a single nondepolarizing collision introduces a change in the y component of velocity of magnitude Δv_y, $\sigma_{\rm eff}^z(t_{21})$ represents an effective cross-section representative of collisions that depolarize *or* produce y-component velocity changes greater than a t_{21}-dependent magnitude, n_0 is the perturber-gas number density when the system is at absolute temperature T, and has internal pressure P_0, $v_{\rm rel}=(8k_bT/\pi\mu)^{1/2}$ is the average echo-atom—perturber-atom relative speed, k_b is the Boltzmann constant, μ is the echo-atom—perturber-atom reduced mass, and $k=k_0$ is the magnitude of the wave vector associated with the optical transition. This description will account for all collisions that occur during t_{32}.

It should be noted that $\sigma_{\rm eff}^z(t_{21})$ has simple asymptotic limits. As $t_{21}\to 0$, the integral over the normalized collision kernel $W(\Delta v_y)$ approaches unity and

$$\sigma_{\rm eff}^z(t_{21}\to 0)=\sigma_D^z\ . \quad (8)$$

On the other hand, if $t_{21}\to\infty$, the integral over Δv_y vanishes and

$$\sigma_{\rm eff}^z(t_{21}\to\infty)=\sigma_D^z+\sigma_{vcc}^z\equiv\sigma_{\rm tot}^z\ . \quad (9)$$

These limits can be understood quite simply. As t_{21} approaches 0, ρ_1^1 and ρ_1^2 are velocity modulated with an ever increasing period, $v_{\rm mod}$. As $v_{\rm mod}$ increases beyond the magnitude of the typical y-component velocity change, collisions become progressively less effective in randomizing the velocity modulation in ρ_1^1 and ρ_1^2. In the $t_{21}\cong 0$ limit, only depolarization effects contribute to echo degra-

dation. On the other hand, when $t_{21}\rightarrow\infty$, $v_{\rm mod}\rightarrow 0$. In this limit, the velocity changes experienced in essentially all nondepolarizing collisions will be large enough to destroy the velocity modulation in ρ_1^1 and ρ_1^2. [This last conclusion follows from the fact that neutral atom-atom collision cross sections are finite which in turn implies $W(0)$ is finite.] Consequently, as $t_{21}\rightarrow\infty$, any collision, whether through its depolarizing or velocity-changing effect, prevents the affected active atom from contributing to the echo signal. In this regime $\sigma_{\rm eff}^z$ represents the total quantum-mechanical scattering cross section, $\sigma_{\rm tot}^z$. For intermediate values of t_{21}, $\sigma_{\rm eff}^z(t_{21})$ represents the cross section for collisions which depolarize *or* produce y-component velocity changes greater than about $v_{\rm mod}/2\pi$.

III. EXPERIMENT

The 556-nm $6s^2\,{}^1S_0$—$6s6p\,{}^3P_1$ transition of the even ($I=0$) isotopes of Yb possess the energy-level scheme shown in Fig. 1. Our experimental apparatus is shown schematically in Fig. 3. The excitation pulses were generated from two pulsed dye lasers pumped by separate excimer lasers. Pulses one, two, and three were, respectively, 3, 3, and 7 nsec in duration, and had spectral widths of 2, 2, and 10 GHz. The delay between pulse one and two (t_{21}) was optically controlled with a modified White Cell optical-delay line,[21] and the delay between pulse two and three (t_{32}) was controlled electronically by adjusting the delay between excimer laser triggers. Our White Cell was constructed from 1- and 2-in-diam mirrors each having a 2-m nominal radius of curvature. The mirrors were dielectrically coated for greater than 99% reflectivity at 556 nm. For the longest delays, it was necessary to use the White Cell in a double-pass configuration. Temporal jitter between excimer pulses was $\lesssim 5$ nsec and was generally much smaller than t_{32} and t_{21}. All pulses were spatially filtered and collimated and were 1—2 mm in diameter. Peak-pulse powers were ~ 10, ~ 20, ~ 200 W for pulses one, two, and three, respectively, although there was some variation from day to day ($\sim 2x$) due to variations in pump power. At short excitation pulse separations, the echo signals were 1% as intense as pulse one. Radiative decay of the $^3P_1$ state (lifetime 875 nsec) resulted in significantly smaller echo signals at the larger pulse separations. Our maximum dynamic range was four decades. The polarization configuration used is the same as discussed above and is shown in Figs. 2 and 3. A small magnetic keeper field of ~ 7 G was applied to the sample along the $\hat{z}$ direction to minimize the effects of stray fields. The energy splitting of the m levels induced by the magnetic field gave rise to quantum-beat-like oscillations in the echo amplitude as a function of excitation-pulse separations (see the Appendix). Since our observations were made in the pressure domain these oscillations did not interfere with our measurements.

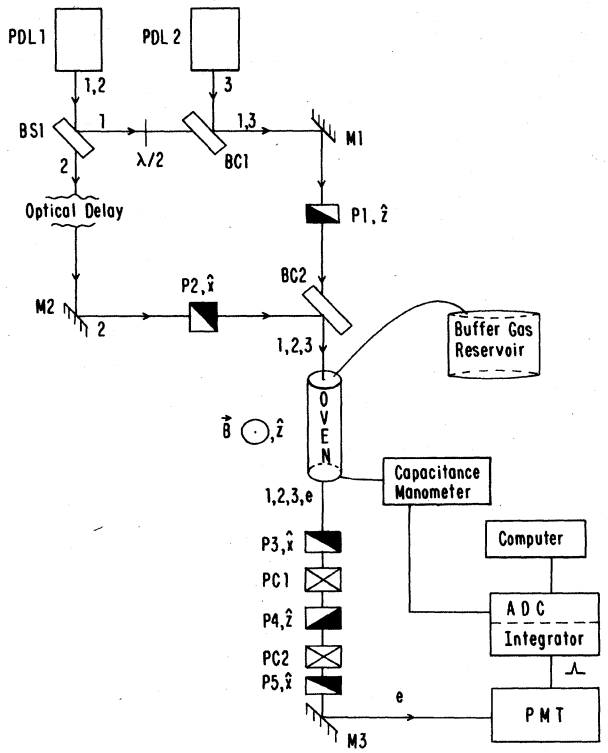

FIG. 3. Schematic of experimental setup. $M1$—$M3$ denote mirrors. BC1 and BC2 are beam combiners. BS1 is a beam splitter. $P1$—$P5$ denote polarizers with the pass axes shown. PC1 and PC2 denote Pockels's cells. $\lambda/2$ denotes a half-wave plate, PDL1 and PDL2 are pulsed-dye lasers, and the paths of pulses one, two, three, and e (echo) are indicated.

The Yb, of natural isotopic composition, was housed in a 25-cm-long stainless-steel heat-pipe-type oven that was maintained at 425 °C. At this temperature the sample was approximately one optical absorption length. The vapor was confined by a small hollow stainless-steel cylindrical can inside the oven. The can, about 10 cm long and 1 cm in diameter, was entirely enclosed except for a 2-mm-diam circular hole at each end that allowed light into the Yb vapor. This confinement scheme was necessary to minimize the strong Yb density variation that otherwise occurred when the buffer-gas pressure was varied. He or Ar perturber gases were bled into the oven from an external reservoir, and the oven pressure was measured with a capacitance manometer and monitored by a computer. Detection of the echo signal was facilitated by a series of Pockel's cell optical shutters that blocked the excitation pulses but allowed the echo to pass through only weakly attenuated. The trilevel echo signal was then directed onto a photomultiplier tube. Single-event photomultiplier tube signals were integrated, digitized, and computer recorded. In a typical experimental run, the excitation-pulse temporal separations are held fixed and the perturber pressure is slowly cycled from low to high values and back, while simultaneously measuring the echo intensity. Results from a sample run are shown in Fig. 4. Each point represents the average of 30 echo signals. The quantity β is determined from the slope of the echo intensity versus pressure data. Measurements of β were made for various values of t_{21} ranging from ~ 14—~ 760 nsec. The interval t_{32} ranged from ~ 0—~ 1200 nsec. For short t_{21}, we could make $t_{32}\gg t_{21}$, and hence $\beta_z\gg\beta_{\rm opt}$. As a result our measurements of β_z are least affected by uncertainty in $\beta_{\rm opt}$ for short t_{21}.

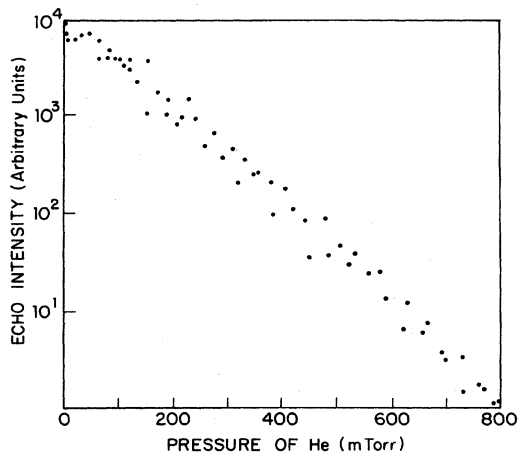

FIG. 4. A scan of echo intensity versus buffer-gas pressure. In this case $t_{21}=55$ nsec and $t_{32}=100$ nsec. For longer t_{21}, t_{32} the signal-to-noise ratio was considerably smaller than shown above.

The frequencies of our dye lasers were set as follows: The broad-bandwidth (10-GHz) laser was simply tuned to maximize the trilevel echo signal. This laser is sufficiently broad to excite essentially the entire Yb-absorption profile (see Fig. 5). The narrow-bandwidth (2-GHz) laser was

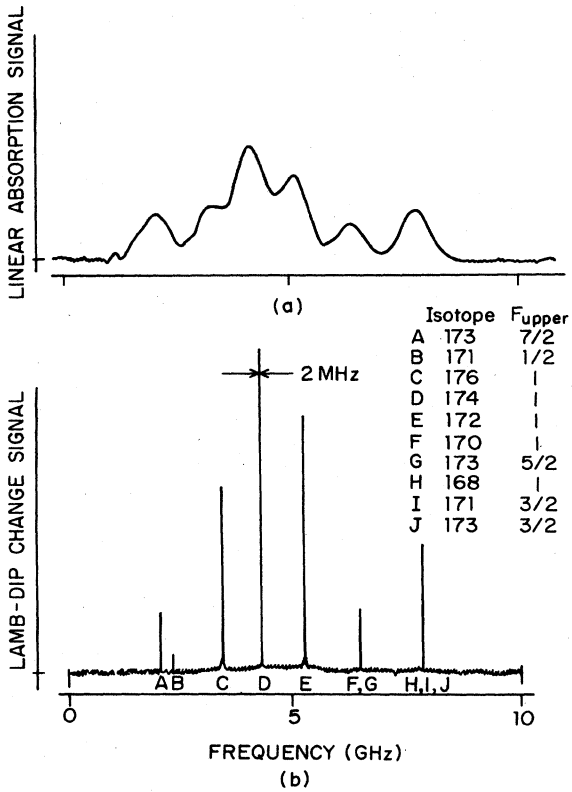

FIG. 5. Absorption of naturally occurring Yb near 5556 Å. (a) is the linear absorption signal, and (b) is a more precise measurement of transition frequency using Lamb dip techniques.[22] The isotopes and transitions corresponding to these lines are indicated. (This figure is reproduced from Ref. 22 with permission.)

piezoelectrically tuned across the absorption profile. The behavior of the trilevel echo intensity was sufficiently similar to the behavior shown in Fig. 5 to allow us to center this laser on the even-isotope (172, 174, 176) portion of the absorption profile.

In order to put an upper bound on the contribution of odd-Yb isotopes to our signal, we performed a series of two-excitation-pulse photon-echo (TPE) experiments. Pulses one and two of the trilevel echo-excitation sequence were used to generate the TPE. In the case of the even isotopes, excitation pulses of orthogonal linear polarization should not produce a TPE. With the dye laser tuned to the frequency used in the actual experiment, the intensity of the TPE's generated by pulses of orthogonal polarization was 100 times weaker than the intensity of TPE's generated with pulses of parallel polarization. When the dye laser was tuned to maximize the contribution of the odd isotopes, the parallel polarization case was favored by a factor of 10. These two observations allow us to conclude that at least 90% of the Yb atoms excited by the narrow-bandwidth laser were even isotopes. This conclusion, however, ignores the fact that imperfections in our optics slightly depolarize our laser pulses and stray magnetic fields depolarize the sample. The latter two effects would also give rise to a TPE signal even if no odd isotopes were excited. While we cannot quantitatively estimate the effect of these factors, we expect them to be significant. It is likely that the actual ratio of even to odd isotopes excited considerably exceeded 10 (see below).

In the case of the trilevel echo, odd isotopes, when excited, contribute to the echo signal through both ground- and excited-state Zeeman coherences. Optical-pumping effects prevent the ground-state coherences from decaying completely even when the excited state undergoes radiative decay. Consequently, long-t_{32} measurements tend to give more weight to the odd-isotope contribution. If odd isotopes actually dominated our signal at long t_{32}, we would expect our measured cross sections to decrease as the ground-state scattering came to dominate the relaxation process. However, no t_{32} dependence of the Zeeman coherence cross sections was observable. These observations lead us to believe that the odd isotopes did not appreciably affect our results.

IV. RESULTS AND DISCUSSION

The effective collision cross sections $\sigma^z_{\rm eff}$ derived from our measurements are presented in Fig. 6. In the case of Yb*-He collisions, our data spans both the short- and long-t_{21} regimes. Hence, we can estimate both σ^z_D(He) and σ^z_{vcc}(He) using, respectively, our shortest and longest t_{21} values of $\sigma_{\rm eff}$. In the case of Yb*-Ar collisions, we can directly estimate σ^z_D(Ar) from our short-t_{21} data; however, since our measurements do not extend into the asymptotic long-t_{21} regime, we can only determine a lower bound for σ^z_{vcc}(Ar). We do this by averaging the long-t_{21} ($\geq$690 nsec) Yb*-Ar data. Values of σ^z_D and σ^z_{vcc} calculated using our short- and long-t_{21} data and Eqs. (7)—(9) are given in Table I.

In addition to the results presented in Table I, our observations of $\sigma^z_{\rm eff}(t_{21})$ also provide information on the

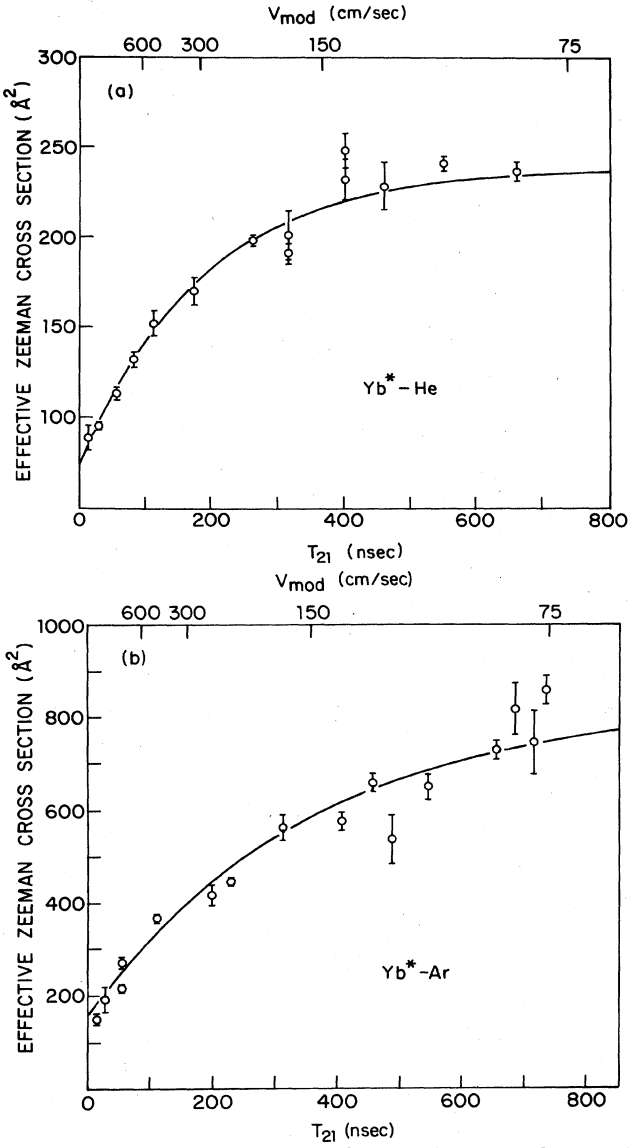

FIG. 6. Measured values of σ^z_{eff} as a function of t_{21}. (a) Yb*-He. (b) Yb*-Ar. Of the three simple kernels considered, the Lorentzian most accurately reproduces our observations. The solid lines are calculated using Lorentzian kernels with the parameters given in Table II. All data points represent an average of 3–8 runs of the type shown in Fig. 4. The error bars represent the standard deviation derived from these runs.

velocity-changing collision kernel $W(\Delta v_y)$, which represents the spectrum of velocity changes experienced by Yb* due to collisions with He or Ar. We have substituted the following three simple functions:

$$W_L(\Delta v_y)=\left[\frac{\delta v_0}{\pi}\right]\left[\frac{1}{(\delta v_0)^2+(\Delta v_y)^2}\right], \tag{10a}$$

$$W_G(\Delta v_y)=(\sqrt{\pi}\,\delta v_0)^{-1}\exp[-(\Delta v_y)^2/(\delta v_0)^2], \tag{10b}$$

$$W_E(\Delta v_y)=(2\,\delta v_0)^{-1}\exp[-|\Delta v_y|/\delta v_0] \tag{10c}$$

into Eq. (7) in an attempt to reproduce the t_{21} dependence of our measured σ^z_{eff}. The accuracy with which these different kernels reproduce our observations gives insight into the structure of the *real* collision kernel which is probably more complicated than any of our simple phenomenological kernels above. The results of these fits are presented in Table II, and are discussed in detail below.

TABLE I. Experimentally derived cross sections. Also presented are other experimental (e) and theoretical (t) estimates of the quantities measured here.

Perturber	σ^z_D (Å²)	σ^z_{vcc} (Å²)	σ_{tot} (Å²)
He	89(7)	150(8)	239(9)
He[a]	92(6)e		220(20)t
Ar	150(10)	≧681(25)	≧836(25)
Ar[b]	167(16)e		

[a] From Refs. 6 and 7.
[b] From Ref. 5. Value here represents an average of alignment and orientation rates measured in Ref. 5.

Agreement between our measured values of $\sigma^z_{\text{eff}}(t_{21})$ and those calculated using Eqs. (7) and (10) was maximized using a weighted least-squares-fitting routine in which σ^z_D, σ^z_{vcc}, and δv_0 were allowed to vary. In the case of He, the number of fitting parameters was only two, since we constrained the sum of σ^z_D and σ^z_{vcc} to equal our measured total scattering cross section (see Table I). The best fitting parameters and reduced χ-square[23] obtained for each fit are given in Table II. The three He fits are compared with our data in Fig. 7. Interestingly, the Gaussian kernel $W_G(\Delta v_y)$, a favorite choice in the analysis of velocity-changing collision work, provides the least satisfactory agreement with our data. This result implies that stronger velocity changes, minimized by the sharp falloff of the Gaussian kernel, play an important role in Yb*-He collisions. This conclusion was also reached in earlier studies of the velocity changes affecting level populations.[24] The Lorentzian kernel $W_L(\Delta v_y)$ comes closest to describing our data, but does not fit the data significantly better than the exponential kernel. In the case of Ar, σ^z_D, σ^z_{vcc}, and δv_0 were allowed to vary independently. Although the Lorentzian kernels reproduced the data more closely than the other kernel types, we found that a wide range of free parameters gave roughly the same quality fit. For example, taking $\sigma^z_D(\text{Ar})=160$ Å², we found that $[\delta v_0, \sigma^z_{vcc}(\text{Ar})]$ ranged from approximately (33 cm/sec, 550 Å²) to (18 cm/sec, 850 Å²) while giving χ-squares within 25% of each other. The fact that a wide range of Lorentzian kernel parameters provide roughly equivalent fits to our data results partially from the presence of scatter in the data. However, it also indicates that the actual Yb*-Ar kernel is more complicated than a simple Lorentzian. The values of δv_0, $\sigma^z_D(\text{Ar})$, $\sigma^z_{vcc}(\text{Ar})$ and the reduced χ-square given in Table II are values corresponding to the best fit Lorentzian kernel.

As described in the Appendix, the echo signal observed in our experiment is sensitive to components of both the orientation (ρ^1_1) and alignment (ρ^2_1) of the $^3P_1$ state. The

TABLE II. Best fit parameters for the indicated phenomenological collision kernels. See text for an explanation of the parameters.

Perturber	Kernel	σ_D^z (Å^2)	σ_{vcc}^z (Å^2)	σ_{tot} (Å^2)	δv_0 (cm/sec)	Reduced χ-square
He	Lorentzian	72	167	239	47	2.39
He	Exponential	91	149	239	59	3.37
He	Gaussian	98	141	239	76	5.82
Ar	Lorentzian	155	679	834	25	7.85

quantities may in general relax at different rates. As a result, Eq. (6) should be generalized [see Eq. (A6)] to represent biexponential decay. We used Eq. (6) to analyze our data, because we were unable to detect any consistent deviation from simple exponential decay in our measurements of echo intensity versus perturber pressure. Since our measurements often extended over several decades of echo intensity, we conclude that ρ_1^1 and ρ_1^2 have very similar relaxation properties in the presence of either depolarizing or velocity-changing collisions. This result is consistent with optical-pumping measurements[25,26] of collisional depolarization.

Collisional relaxation in the $6s\,6p\ ^3P_1$ Zeeman manifold has also been studied by Keller and Le Gouët.[6,7,27] They employed a stimulated photon-echo technique which in many respects is similar to the trilevel echo technique reported here. In particular, they also employ a pair of excitation pulses to generate a velocity-modulated excitation of the $^3P_1$ state. A third excitation pulse (in their case resonant with a different optical transition) generates an echo signal that is sensitive to the collisional perturbations of the $^3P_1$ state. As in the present experiment, they can change their sensitivity to collisional velocity changes by varying the temporal separation t_{21} between the first two excitation pulses. Keller's and Le Gouët's experiment, however, is sensitive to the relaxation of the spherical tensors ρ_0^0 (proportional to the total population in the $^3P_1$ state) and ρ_0^2 (a component of alignment). By studying the relaxation of echo signals generated with different excitation polarizations, they were able to isolate the relaxation rate associated with ρ_0^0. We have converted the results of their Yb*-He collision measurements to our units, and compared their data with our short-t_{21} data in Fig. 8. For longer values of t_{21}, the data sets converge, suggesting that the various tensor moments relax identically when the effects of sufficiently weak velocity changes are included. For shorter values of t_{21}, their relaxation cross sections fall below ours. This behavior is reasonable since ρ_0^0 is not subject to collisional depolarization, and as t_{21} approaches zero, fewer and fewer velocity changes are large enough to destroy the velocity modulation initially created in ρ_0^0.

As noted above, the collision cross sections measured here and in the experiment of Keller and Le Gouët seem to become approximately equal when t_{21} is greater than some value t_c. A very naive model which uses our measured value of σ_D^z provides us with a rough estimate of t_c. We assume that σ_D^z represents the total cross section for collisions which affect the various tensor moments differently, i.e., collisions with impact parameters outside a disk of area σ_D^z centered about the scattering center are assumed to affect all tensor moments identically. We note that collisions which affect higher-rank tensor moments by depolarization will affect the rank-zero tensor moment by velocity thermalization. We estimate the *smallest* velo-

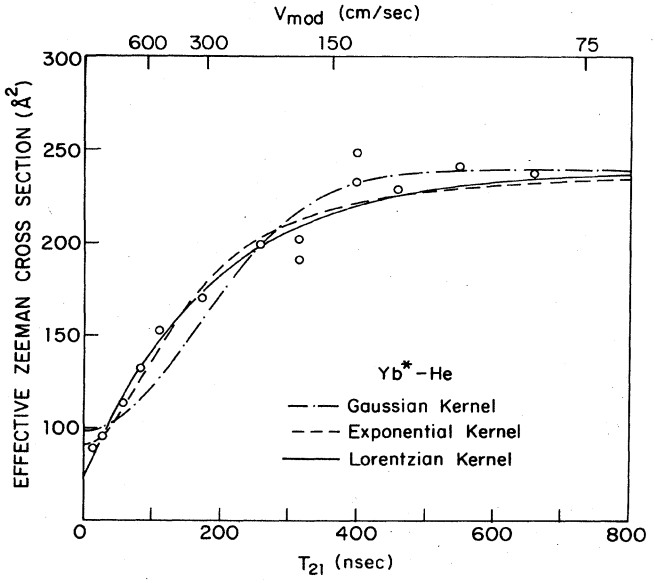

FIG. 7. A comparison of the observed variation of σ_{eff}^z with t_{21} and that predicted on the basis of the three kernels of Table II.

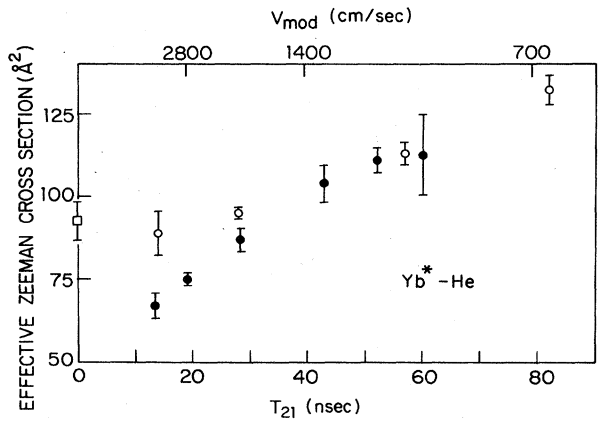

FIG. 8. Our short t_{21}, Yb*-He experimental data (○) along with the stimulated-echo experimental data of Refs. 6 and 7 (●). We have also included σ_D^z(He) as measured in Ref. 7 (□). See text for discussion.

city change, $v_D^{\min}$, occurring in *depolarization-type* collisions by considering diffractive scattering[28] from a hole of area σ_D^z. We find that

$$v_D^{\min}=\frac{2(\pi)^{1/2}\hbar}{M(\sigma_D^z)^{1/2}}\ , \tag{11}$$

where M is the Yb atomic mass. As mentioned above, $\sigma_{\rm eff}^z(t_{21})$ represents the effect of collisional depolarization *and* collisional velocity changes of magnitude *greater than* $v_{\rm mod}/2\pi=\lambda_0/2\pi t_{21}$. When t_{21} is sufficiently large that $\sigma_{\rm eff}^z(t_{21})$ is sensitive to all depolarization-type collisions *either* through their depolarization *or* through their velocity thermalization effect, $\sigma_{\rm eff}^z$ should be the same for all spherical tensors. By setting $v_D^{\min}=v_{\rm mod}/2\pi$, we conclude that

$$t_c\approx\frac{\lambda_0}{2\pi v_D^{\min}}\ . \tag{12}$$

In the case of Yb*-He collisions Eqs. (11) and (12) give, respectively, $v_D^{\min}\cong 130$ cm/sec and $t_c\cong 65$ nsec. The latter value is close to the value of t_{21} at which our cross sections and Keller and Le Gouët's cross sections converge. For $t_{21}>t_c$, we expect that the cross sections reported here and in Ref. 27 will have essentially the same values.

V. SUMMARY

In conclusion, we have presented a comprehensive set of data which characterizes the relaxation of $6s\,6p\ ^3P_1$ Yb Zeeman coherences resulting from collisions involving He and Ar perturbers. These measurements are among the first involving Zeeman coherences that are sensitive to both depolarizing and velocity-changing effects. Comparing our results with those of others,[6,7] we have found evidence that various tensor moments may relax identically when the effects of depolarization *and* velocity changes on the order of $v_D^{\min}$ and larger, are both included. This conclusion follows from the convergence of the cross sections shown in Fig. 8. In the case of He, the velocity-change spectrum is simulated quite well by a Lorentzian-type kernel, while that of Ar appears to be more complicated. The Yb velocity changes induced by both He and Ar are both found to be largely characteristic of diffractive scattering, i.e. the characteristic magnitude of the velocity change active can be estimated on the basis of simple geometric considerations without resorting to detailed potential scattering calculations.

ACKNOWLEDGMENTS

One of us (A.G.Y.) gratefully acknowledges financial support from the U.S. Army Research Office, Grant No. DAAG19-83-0008. Financial support for this work was provided by the National Science Foundation under Grant No. PHY-82-07080, and by the U.S. Joint Services Electronics Program under Contract No. N00014-84-K-0415.

APPENDIX

It is well known that the statistical properties of a Zeeman manifold can be calculated using a density matrix ρ which, in the $|J,M\rangle$ representation, is defined as

$$\rho=\sum_{M',M}\langle J,M'|\rho|J,M\rangle\,|J,M'\rangle\langle J,M|\ . \tag{A1}$$

Here $|M'|$, $|M|\le J$ and the sum is over all allowed values of M' and M. When angular symmetries of the ensemble described by ρ are of interest, it is convenient to expand ρ in terms of irreducible tensor operators or spherical tensors denoted by $[T(J,J)]_{KQ}$, i.e.,[3,29]

$$\rho=\sum_{K,Q}\rho_Q^K(J,J)[T(J,J)]_{KQ} \tag{A2}$$

where K denotes the rank and Q the component of the spherical tensor. The coefficient of each spherical tensor operator, $\rho_Q^K(J,J)$, is called a state multipole and is derived from ρ using the formula below:

$$\rho_Q^K(J,J)=\sum_{M',M}(-1)^{J-M'}(2K+1)\times\begin{bmatrix}J & J & K\\ M' & -M & -Q\end{bmatrix}\langle J,M'|\rho|J,M\rangle\ , \tag{A3}$$

where

$$\begin{bmatrix}J & J & K\\ M' & -M & -Q\end{bmatrix}$$

is a 3-j symbol. In general, the collisional decay of a coherence can be described in terms of the independent relaxation of various spherical tensor multipoles associated with that coherence.

The state multipoles associated with the Zeeman coherences created in the $^3P_1$ state by the first two excitation pulses can be computed from using Eq. (A3), with $J=1$. Thus it can be shown that during t_{32}, the excited state has eight nonzero-state multipoles associated with it. They are

$$\rho_0^0=\frac{1}{\sqrt{3}}\left[\cos^2\left[\frac{\theta_1}{2}\right]\sin^2\left[\frac{\theta_2}{2}\right]+\sin^2\left[\frac{\theta_1}{2}\right]\right], \tag{A4a}$$

$$\rho_0^2=\frac{1}{\sqrt{6}}\left[\cos^2\left[\frac{\theta_1}{2}\right]\sin^2\left[\frac{\theta_2}{2}\right]-2\sin^2\left[\frac{\theta_1}{2}\right]\right], \tag{A4b}$$

$$\rho_{+2}^2=\rho_{-2}^{2*}=\frac{-1}{2}\cos^2\left[\frac{\theta_1}{2}\right]\sin^2\left[\frac{\theta_2}{2}\right]\exp\left[i2\Delta\omega\left[t-t_2-\mathbf{k}_2\cdot\frac{(\mathbf{r}_2-\mathbf{r}_0)}{c}\right]\right], \tag{A4c}$$

$$\rho^2_{+1}=-\rho^{2*}_{-1}=\cos\left[\frac{\theta_1}{2}\right]\sin\left[\frac{\theta_1}{2}\right]\sin\left[\frac{\theta_2}{2}\right]\cos[\omega_0 t_{21}+v_y k_0 t_{21}+(\varphi_1-\varphi_2)]\exp\left[-i\,\Delta\omega\left[t-t_2-\hat{\mathbf{k}}_2\cdot\frac{(\mathbf{r}_2-\mathbf{r}_0)}{c}\right]\right]$$

$$=(\rho^2_{+1})_0\exp\left[-i\,\Delta\omega\left[t-t_2-\hat{\mathbf{k}}_2\cdot\frac{(\mathbf{r}_2-\mathbf{r}_0)}{c}\right]\right], \tag{A4d}$$

$$\rho^1_{+1}=-\rho^{1*}_{-1}=-i\cos\left[\frac{\theta_1}{2}\right]\sin\left[\frac{\theta_1}{2}\right]\sin\left[\frac{\theta_2}{2}\right]\sin[\omega_0 t_{21}+v_y k_0 t_{21}+(\varphi_1-\varphi_2)]\exp\left[-i\,\Delta\omega\left[t-t_2-\hat{\mathbf{k}}_2\cdot\frac{(\mathbf{r}_2-\mathbf{r}_0)}{c}\right]\right]$$

$$=(\rho^1_{+1})_0\exp\left[-i\,\Delta\omega\left[t-t_2-\hat{\mathbf{k}}_2\cdot\frac{(\mathbf{r}_2-\mathbf{r}_0)}{c}\right]\right]. \tag{A4e}$$

Here the derivation of the excited-state density matrix followed the general method given in Ref. 19, but is expressed in the laboratory frame.

If we express the density matrix at the echo time in terms of these excited-state multipoles, we can determine the spherical tensors to which the echo polarization is sensitive. We did this and found that

$$P_{\text{echo}}(t,v_y,y)\propto\{(\rho^2_1)_0\sin[\omega_0(t-t_3)-k_0(y-y_0)+k_0v_y(t-t_3)+\varphi_3]$$
$$+(\rho^1_1)_0\cos[\omega_0(t-t_3)-k_0(y-y_0)+k_0v_y(t-t_3)+\varphi_3]\}\cos\left[\Delta\omega(t-t_2)+\frac{\Delta\omega}{c}[y-y_0-v_y(t-t_2)]\right] \tag{A5a}$$

or, substituting for $(\rho^2_1)_0$ and $(\rho^1_1)_0$

$$P_{\text{echo}}(t,v_y,y)\propto 2\cos\left[\Delta\omega(t-t_2)+\frac{\Delta\omega}{c}[y-y_0-v_y(t-t_2)]\right]$$
$$\times\sin[\Delta\omega(t_{21}+t_3-t)+k_0(y-y_0)+k_0v_y(t_{21}+t_3-t)+\varphi_1-\varphi_2-\varphi_3], \tag{A5b}$$

where $\Delta\omega$ is the splitting between adjacent m levels.

As is easily seen from Eqs. (A5), at $t\cong t_e=t_3+t_{21}$, the polarization $P_{\text{echo}}(t,v_y,y)$, becomes essentially independent of velocity. At this time, all velocity groups in the sample add constructively to create a macroscopic polarization. This can be demonstrated explicitly by integrating (A5) over v_y. The macroscopic polarization at $t\cong t_e$ gives rise to our trilevel echo. The echo is sensitive to the $K=1$ (orientation) and $K=2$ (alignment) rank spherical tensors. Since we expect moments of different rank K to relax at distinct rates, the degradation of our echo intensity [proportional to the optical cycle average of the square of Eq. (A5a)] as a function of perturber pressure P will in general be the sum of two different exponentials, i.e.,

$$I_e(P)\propto|(\rho^2_1)_0|^2\exp(-\beta^{(2)}_z P)+|(\rho^1_1)_0|^2\exp(-\beta^{(1)}_z P), \tag{A6}$$

where $\beta^{(k)}_z$ is associated with the Kth-rank contribution to the signal. Relaxation of the optical coherence [see Eq. (6)] results in a multiplicative exponential factor in both terms above.

Despite the fact that our experiment measures a superposition of alignment and orientation decay, the data obtained here can be used in conjunction with data from trilevel echo experiments performed with different excitation-pulse polarizations to unambiguously determine the individual orientation and alignment decay rates.

[1]W. Happer, Rev. Mod. Phys. **44**, 169 (1972), and references therein.

[2]U. Fano, Rev. Mod. Phys. **29**, 74 (1957).

[3]A. Omont, *Progress in Quantum Electronics* (Pergamon, London, 1977), Vol. 5, p. 69.

[4]A. Omont, J. Phys. (Paris) **26**, 576 (1965).

[5]A. P. Ghosh, C. D. Nabors, M. A. Attili, J. E. Thomas, and M. S. Feld, Phys. Rev. Lett. **53**, 1333 (1984), and private communication.

[6]J. C. Keller and J. L. Le Gouët, Phys. Rev. Lett. **52**, 2034 (1984).

[7]J. L. Le Gouët and J. C. Keller, in Proceedings of the Seventh International Conference on Spectral Lineshapes, Aussois, France, 1984 (unpublished).

[8]I. Colomb and M. Dumont, Opt. Commun. **21**, 143 (1977).

[9]I. Colomb, M. Gorlicki, and M. Dumont, Opt. Commun. **21**, 289 (1977).

[10]P. R. Berman, Adv. At. Mol. Phys. **13**, 57 (1977), and references therein.

[11]P. R. Berman, Phys. Rep. **43**, 101 (1978).

[12]J. L. Le Gouët and P. R. Berman, Phys. Rev. A **24**, 1831 (1981).

[13]P. R. Berman, Lectures presented at the 1982 Summer School at Les Houches, France (North-Holland, Amsterdam, 1984).

[14]P. R. Berman, T. W. Mossberg, and S. R. Hartmann, Phys. Rev. A **25**, 1550 (1982).

[15]R. A. Forber, L. Spinelli, J. E. Thomas, and M. S. Feld, Phys. Rev. Lett. **50**, 331 (1983).

[16]P. R. Berman, J. M. Levy, and R. G. Brewer, Phys. Rev. A **11**, 1668 (1975).

[17]B. Comasky, R. E. Scotti, and R. L. Shoemaker, Opt. Lett. **6**, 45 (1981).

[18]J. E. Thomas, R. A. Forber, L. A. Spinelli, and M. S. Feld, Phys. Rev. Lett. **51**, 2194 (1983).

[19]T. W. Mossberg, R. Kachru, S. R. Hartmann, and A. M. Flusberg, Phys. Rev. A **20**, 1976 (1979); for a simple picture of echo formation see T. W. Mossberg and S. R. Hartmann, Phys. Rev. A **23**, 1271 (1981).

[20]T. W. Mossberg, E. Whittaker, R. Kachru, and S. R. Hartmann, Phys. Rev. A **22**, 1962 (1980); T. W. Mossberg, R. Kachru, K. P. Leung, E. Whittaker, and S. R. Hartmann, in *Spectral Line Shapes* (de Gruyter, New York, 1981), p. 1093.

[21]J. U. White, J. Opt. Soc. Am. **32**, 285 (1942).

[22]R. A. Forber, Ph.D. thesis, Massachusetts Institute of Technology, 1983 (unpublished).

[23]P. R. Bevington, *Data Reduction and Error Analysis for the Physical Sciences* (McGraw-Hill, New York, 1969).

[24]T. Mossberg, A. Flusberg, R. Kachru, and S. R. Hartmann, Phys. Rev. Lett. **42**, 1665 (1979).

[25]J. P. Faroux and J. Brossel, C. R. Acad. Sci. **263B**, 612 (1966).

[26]J. P. Barrat, D. Casalta, J. L. Cojan, and J. Hamel, J. Phys. Paris **27**, 608 (1966).

[27]J. C. Keller and J. L. Le Gouët (unpublished). We thank these authors for a prepublication copy of their manuscript. This manuscript describes their procedure in the greatest detail.

[28]Equation (11) is derived using the angle at which the far-field scattered intensity of a plane wave diffracting through a circular aperture of area σ_D^2 falls off by a factor of $1/e$. This is clearly somewhat arbitrary.

[29]K. Blum, *Density Matrix Theory and Applications* (Plenum, New York, 1981).